CHAPTER VI

DISTRIBUTION FUNCTIONS

In the next two chapters we examine in more detail the agreement between experiment and the predictions of the models discussed previously. We focus on those properties which should distinguish among different classes of systems. We examine, in particular, the distributions of number of sides and area, and the correlation between area and number of sides and between the number of sides of neighboring bubbles. Because of the large uncertainties in the experimental measurements our conclusions will be indicative rather than definitive.

Besides the mean bubble area, the two basic measures of the state of a froth are the distribution of the number of sides, $\rho(n)$, the probability a randomly selected bubble has n sides, and the normalized area distribution, $\rho(A/ < a >)$, the probability that a bubble has an area which is a given fraction of the mean bubble area. Such measurements have been made even in systems for which the dynamics are not well studied. A typical example is three dimensional grain growth in a metal, where measurement of the size distribution usually involves sectioning and hence precludes measurements in time.

A basic problem with any distribution function measured in a finite area is that large bubbles are more likely to touch the area's boundary (and hence to be excluded from the statistics) than are small bubbles. We therefore have a systematic bias against large (and many-sided) bubbles in our distribution

functions and their moments. To the accuracies that we are able to measure, this error is not significant, but we have given two examples of corrected distributions in Table 7 and 8. For the second moment, the effective correction is of the order of 5%. It is relatively smaller for higher moments. The mathematics of distribution function correction is discussed in detail in Miles, Lantuejoul and Blanc and Mocellin.[30,137,166]

VI.a Side Distributions

We define the mth moment of the side distribution as:

$$\mu_m \equiv \sum_{n=2}^{\infty} \rho(n)(n - < n >)^m, \qquad \text{VI.1}$$

and the width of the distribution,

$$W \equiv \sum_{n=2}^{\infty} \rho(n)|n - < n > |. \qquad \text{VI.2}$$

For experimental distributions, $< n >$ may differ from six so our calculated values for the moments may differ slightly from those given elsewhere. The larger the difference between $< n >$ and six, the less reliable the distribution and the larger the error in the moment estimate. Moments higher than μ_2 are sensitive to the large n tail of the distribution, which is hard to measure, and thus are frequently only useful as qualitative indicators. W is useful because it is much less sensitive to small counting error fluctuations for large n than are the higher moments. We will also refer to the ratio $\mathcal{R} \equiv \frac{\rho(5)}{\rho(6)}$, another simple reduction of the distribution.

While there are no general rules for correcting for statistical errors, we find that small sample sizes tend to reduce average moments. For example, if

there is a nominal 1% probability for twelve-sided bubbles, the contribution to μ_2 should be 0.36, which we shall see is a large effect. With a typical sample of thirty bubbles, however, we will usually not see any twelve-sided bubbles, and our estimate of μ_2 will be correspondingly low. The problem is worse for higher moments. Occasionally we will attempt to correct for this bias by averaging several distributions, but most of the time we do not have multiple samples to average.

Let us begin our discussion by examining the typical evolution of the side distribution for two dimensional soap bubble coarsening. In Fig. 33 we plot Glazier *et al.*'s data for the directly digitized air froth shown in Fig. 17, which began a well ordered pattern with a side distribution sharply peaked at six. As a function of time, they observed a monotonic decrease in the fraction of six-sided bubbles $\rho(6)$ and a monotonic increase in the fraction of five-sided bubbles, $\rho(5)$. The large n tail of the distribution first broadened, then narrowed to an equilibrium width. At long times, just after the rate of evolution rolled over to a power law ($t > 10,000$ minutes) they observed an essentially time independent distribution function, with $\mathcal{R} = 1.03$, implying the existence of a scaling state. We may see this scaling state more clearly in Fig. 34 (from Stavans and Glazier, taken from the helium froth shown in Figs. 16 (d) and 9 (left)). In this figure, Glazier and Stavans have superimposed the side distributions for three different times

Fig. 33 $\rho(n)$ versus Time. Side distribution versus time for an initially ordered air froth. In order of decreasing $\rho(6)$, measurement times were: $t = 0$ minutes, $t = 545$ minutes, $t = 1124$ minutes, $t = 1565$ minutes, $t = 2044$ minutes, and $t = 3163$ minutes. Note that the distribution first broadens and then narrows to its equilibrium shape (From Glazier *et al.* 1989).[93]

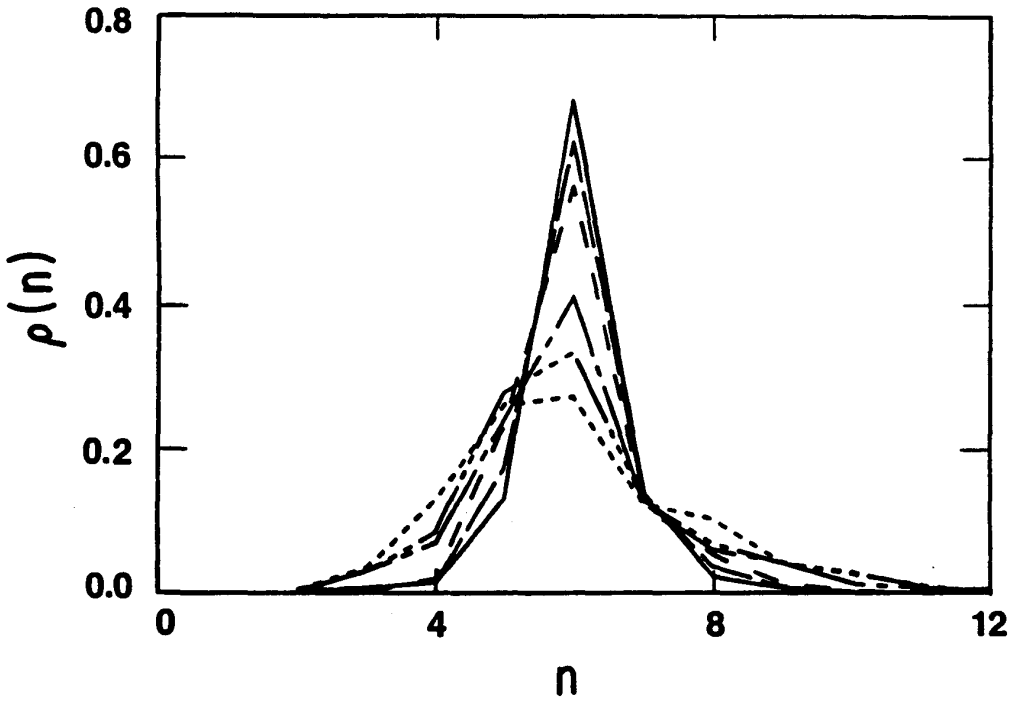
0.8
0.6
0.4
0.2
0.0
ρ(n)
0
4
8
12
n

Fig. 34 $\rho(n)$ versus Time. Side distribution versus time for an initially ordered two dimensional helium froth. Taken at three different times in the scaling regime: $t = 15.25$ hours (open circles), $t = 29.48$ hours (solid circles), and $t = 32.9$ hours (crosses). Number of bubbles ranges from a few hundred to about sixty (From Stavans and Glazier 1989).[220]

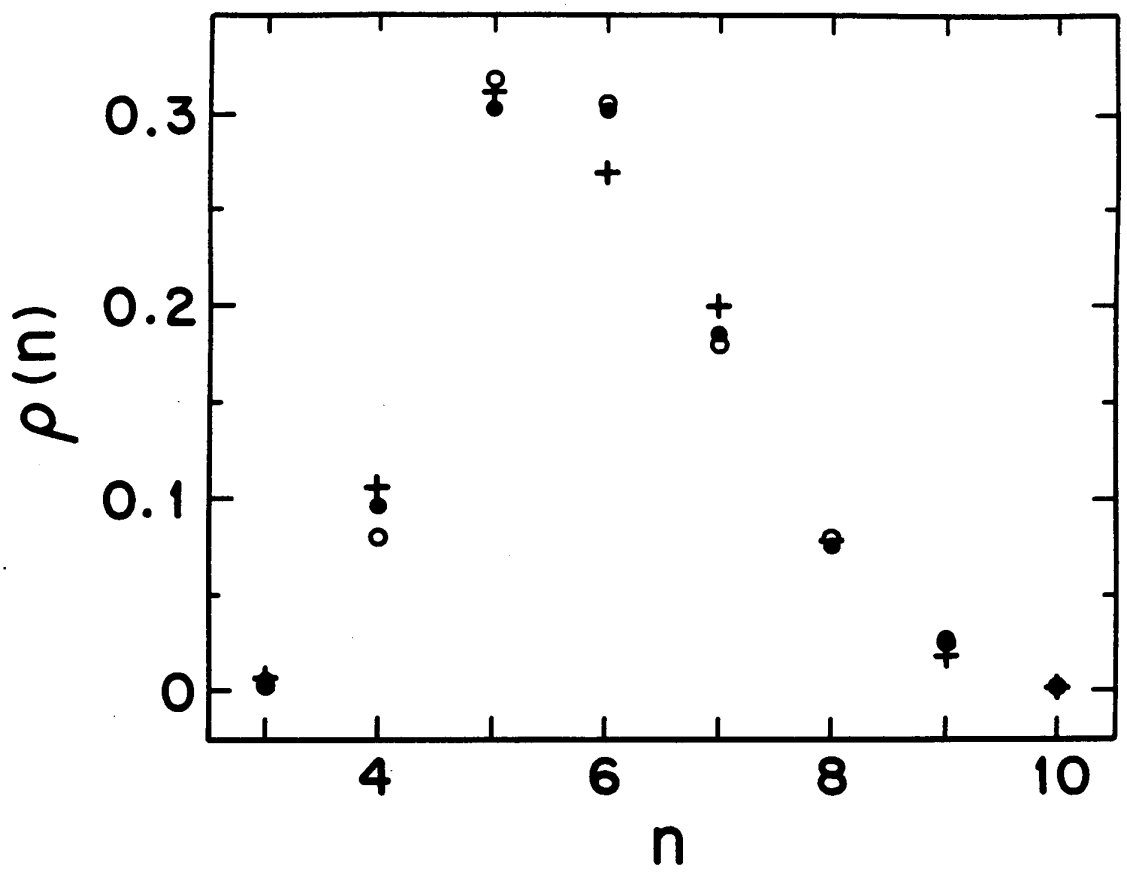
0.3
0.2
0.1
0
ρ(n)
4
6
8
10
n

Fig. 35 Side Distributions. Side distribution for the scaling state of an initially disordered two dimensional air froth (solid) and for the $Q = 48$ hexagonal lattice, nearest neighbor Potts model (dashed) (From Glazier *et al.* 1989).[93]

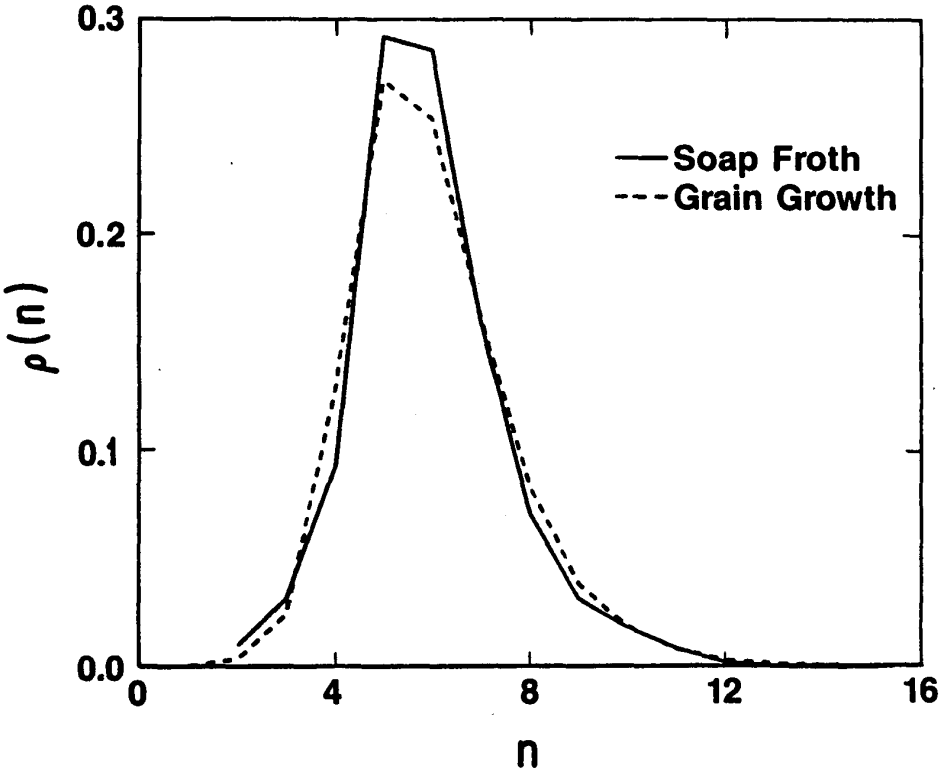
0.3
0.2
0.1
0.0
ρ(n)
0
4
8
12
16
n
Soap Froth
Grain Growth

Fig. 36 μ_2 versus Time. Second moment of the side distribution versus time for an initially ordered helium froth (dots), and an initially disordered air froth (circles). The time scale of the initially ordered run has been multiplied by three (From Stavans and Glazier 1989).[220]

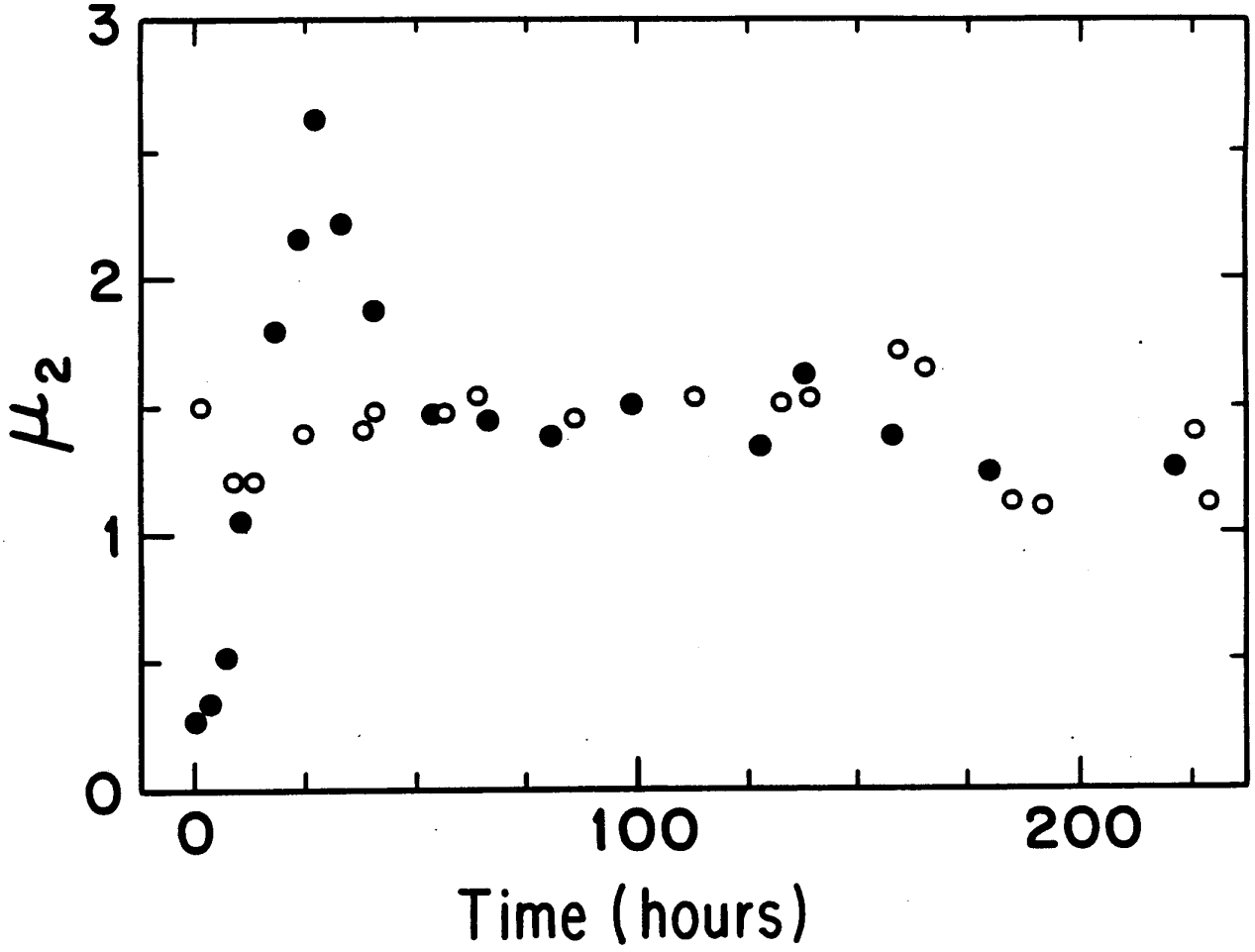
3
2
1
0
μ_2
0
100
200
Time (hours)

Fig. 37 μ_2 versus Time. Second moment of the side distribution versus time for two dimensional initially ordered air froth (From Glazier *et al.* 1989).[93]

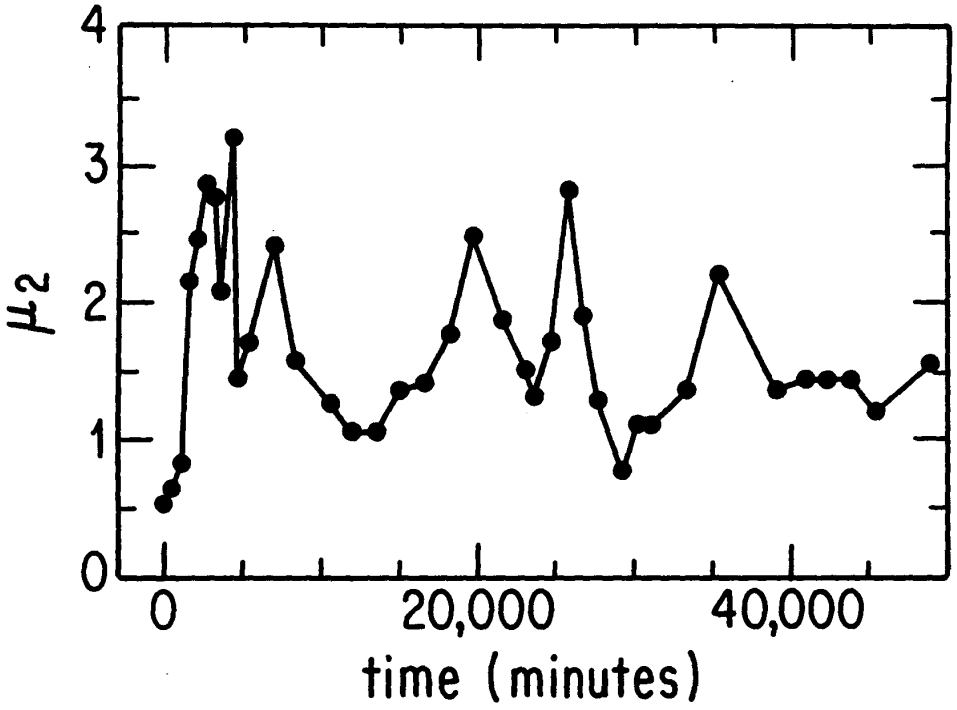
4
3
2
1
0
μ_2
0
20,000
40,000
time (minutes)

Fig. 38 μ_3 versus Time. Third moment of the side distribution versus time for two dimensional initially ordered air froth (From Glazier *et al.* 1989).[93]

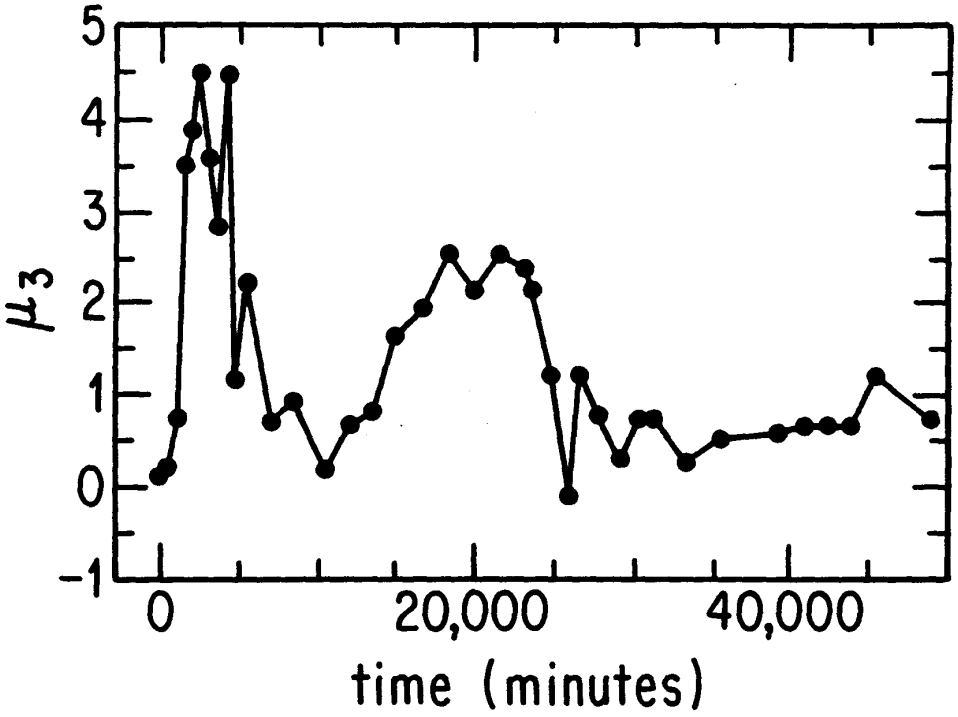
5
4
3
2
1
0
-1
μ_3
0
20,000
40,000
time (minutes)

Fig. 39 μ_4 versus Time. Fourth moment of the side distribution versus time for two dimensional initially ordered air froth (From Glazier *et al.* 1989).[93]

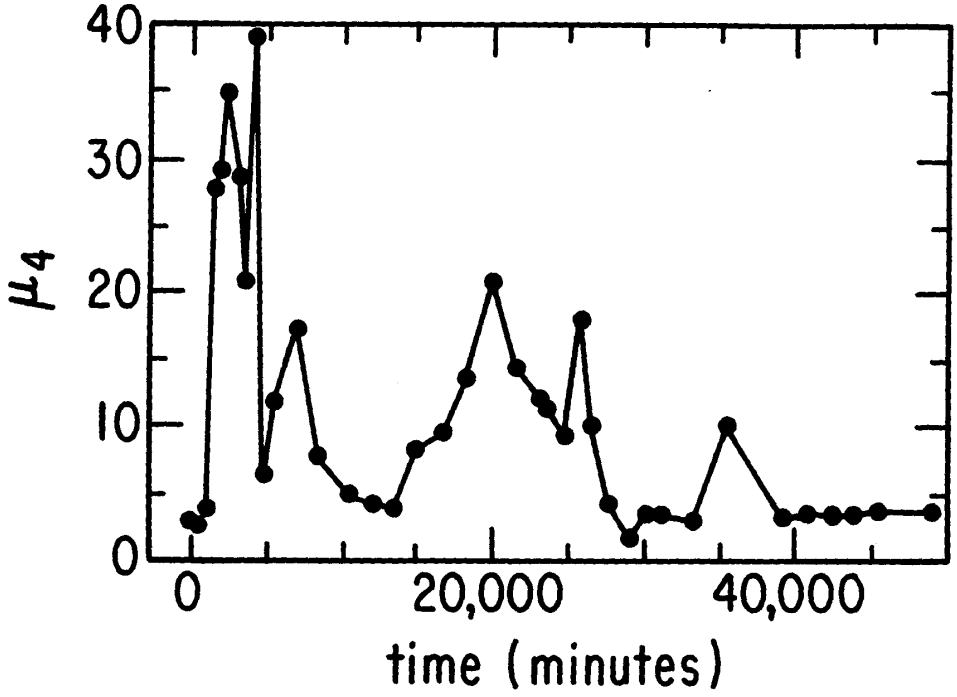
40
30
20
10
0
μ_4
0
20,000
40,000
time (minutes)

Fig. 40 W versus Time. Width of the side distribution versus time for two dimensional initially ordered air froth (From Glazier *et al.* 1989).[93]

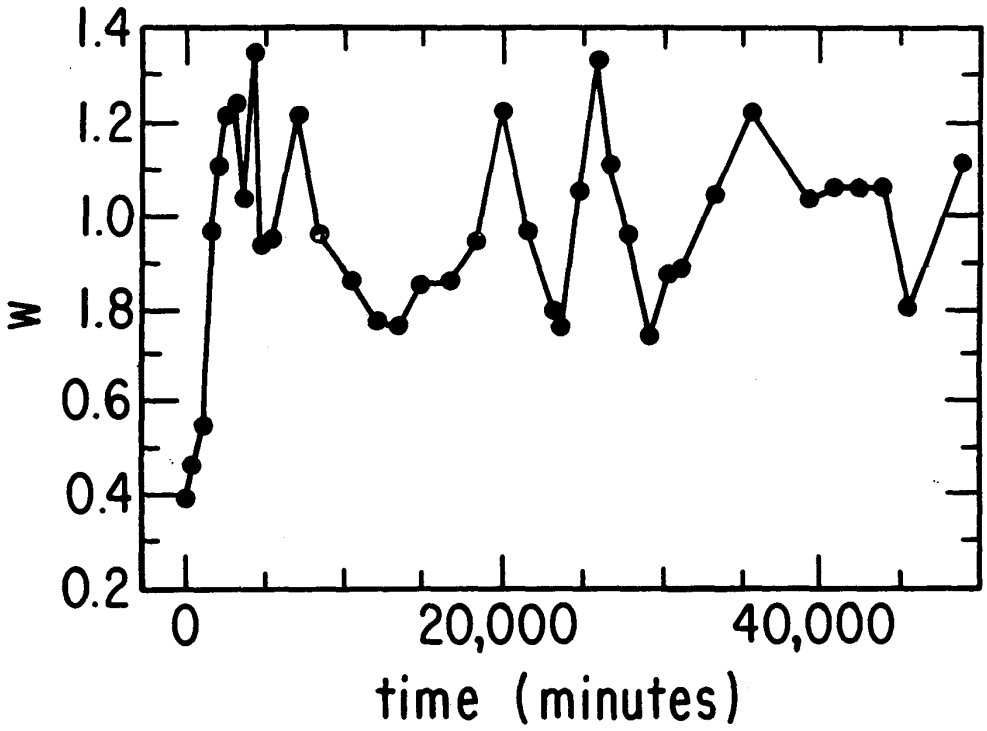
1.4
1.2
1.0
1.8
0.6
0.4
0.2
W
0
20,000
40,000
time (minutes)

TABLE 7

SIDE DISTRIBUTION FUNCTIONS

System	$\rho(3)$ ($\rho(10)$)	$\rho(4)$ ($\rho(11)$)	$\rho(5)$ ($\rho(12)$)	$\rho(6)$ ($\rho(13)$)	$\rho(7)$ ($\rho(14)$)	$\rho(8)$ ($\rho(15)$)	$\rho(9)$ ($\rho(16)$)
Experiment							
Two D Soap Froth							
Smith[206]							
Air[206]	0.01	0.08	0.27	0.35	0.18	0.11	
Air[121]	0.018 (0.009)	0.096 (0.0006)	0.282	0.318	0.161	0.083	0.031
±	0.009 (0.009)	0.043 (0.0006)	0.032	0.036	0.025	0.025	0.021
Aboav[8]							
$t = 0$h $N = 4612$	-	-	0.126	0.731	0.112	0.001	
$t = 0$h $N = 5687$	0.002	0.022	0.212	0.537	0.204	0.022	0.001
$t = 15$h $N = 3550$	0.012 (0.0003)	0.050 (0.0003)	0.217	0.461	0.206	0.050	0.004
$t = 30$h $N = 3623$	0.011 (0.001)	0.059 (0.0006)	0.265 (-)	0.373 (0.0003)	0.198	0.074	0.018
$t = 75$h $N = 1372$	0.026 (0.011)	0.080 (0.004)	0.284 (0.0007)	0.308 (0.0007)	0.174	0.077	0.035
$t = 105$h $N = 584$	0.034 (0.017)	0.111 (0.010)	0.291 (0.010)	0.262 (0.003)	0.149	0.077	0.033 $[\rho(18)]$ [0.002]

TABLE 7, *continued*

System	$\rho(3)$ ($\rho(10)$)	$\rho(4)$ ($\rho(11)$)	$\rho(5)$ ($\rho(12)$)	$\rho(6)$ ($\rho(13)$)	$\rho(7)$ ($\rho(14)$)	$\rho(8)$ ($\rho(15)$)	$\rho(9)$ ($\rho(16)$)
Experiment							
Two D Soap Froth							
Glasier *et al.*							
Air[93]	0.032	0.093	0.292	0.285	0.159	0.072	0.032
	(0.018)	(0.018)	(0.002)				
Air[94]	0.003	0.102	0.277	0.329	0.201	0.073	0.009
$N = 343$	(0.009)	(0.003)					
$N = 111$	0.000	0.090	0.333	0.315	0.144	0.072	0.045
Helium[94]	0.004	0.101	0.321	0.314	0.137	0.058	0.041
$N = 1696$	(0.017)	(0.008)	(0.003)	(0.002)			
$N = 423$	0.000	0.071	0.333	0.298	0.187	0.073	0.038
	0.003	0.090	0.325	0.289	0.193	0.064	0.032
$N = 311$	(0.003)						
Average of	0.010	0.091	0.314	0.305	0.170	0.069	0.033
Above	(0.008)	(0.005)	(0.0008)	(0.0003)			
$\pm$	0.013	0.011	0.023	0.017	0.027	0.006	0.013
	(0.008)	(0.007)	(0.001)	(0.0007)			
Metal Grains							
Al $+10^{-4}$ Mg .22mm Foil[75]							
$T = 0$	0.031	0.153	0.252	0.252	0.156	0.078	0.044
	(0.016)	(0.012)	(0.002)	(0.003)	(–)	(0.003)	
$T = 1.5$h	0.034	0.153	0.274	0.254	0.161	0.090	0.033
							[$\rho(2)$]
	(0.015)	(0.006)					[0.003]
$T = 3.25$h	0.031	0.134	0.275	0.241	0.161	0.078	0.037
	(0.022)	(0.008)					
$T = 4.25$h	0.045	0.120	0.236	0.236	0.152	0.084	0.032
	(0.026)	(0.009)	(0.006)	(0.007)	(0.005)	(0.003)	[0.003]
Averaged	0.035	0.140	0.259	0.246	0.157	0.082	0.036
	(0.020)	(0.009)	(0.002)	(0.0025)	(0.0012)	(0.0013)	[0.0016]
$\pm$	0.002	0.007	0.016	0.019	0.009	0.005	0.006
	(0.005)	(0.003)	(0.003)	(0.003)	(0.002)	(0.002)	[0.002]

TABLE 7, *continued*

System	$\rho(3)$ ($\rho(10)$)	$\rho(4)$ ($\rho(11)$)	$\rho(5)$ ($\rho(12)$)	$\rho(6)$ ($\rho(13)$)	$\rho(7)$ ($\rho(14)$)	$\rho(8)$ ($\rho(15)$)	$\rho(9)$ ($\rho(16)$)
			Experiment				
Biological							
Cucumber[142]	–	0.023	0.265	0.445	0.231	0.035	0.003
Dividing[147]	–	–	0.016	0.255	0.478	0.224	0.026
	(0.001)						
Eupatorium[147]	–	0.026	0.265	0.436	0.238	0.034	0.001
Human Amnion[142]	0.004	0.054	0.248	0.397	0.241	0.049	0.007
Mouthbreeder Fish[105]	–	–	0.214	0.643	0.143		
Rock Fracture							
Pieri[191]							
Basalts							
Giant's Causeway	–	0.040	0.347	0.507	0.081	0.024	
Devil's Postpile	0.025	0.091	0.368	0.440	0.076		
Mt. Rodeix	–	0.148	0.499	0.328	0.024		
Devil's Tower	–	0.169	0.422	0.354	0.055		
Europa Type 1,2	0.038	0.171	0.4623	0.2517	0.078		
Coörd # 4							
Circle Cliffs	0.329	0.624	0.048				
Zendan, Iran	0.406	0.524	0.061	0.008			
Colorado	0.324	0.656	0.020				
Europa Type 3	0.404	0.463	0.124	0.008			
Europa Mixed	0.182	0.491	0.243	0.074	0.002	0.007	
Other 2 D							
Photo Emulsion[142]	0.031	0.222	0.253	0.171	0.129	0.070 [$\rho(17)$]	0.053 [$\rho(19)$]
$N = 1000$	(0.034)	(0.019)	(0.009)	(0.004)	(0.001)	[0.001]	[0.001]
Lipid Monolayers							
Stearic Acid[169]	0.071	0.125	0.269	0.269	0.125	0.089	–
	(0.035)	(–)	(–)	(0.018)			
Pentadecanoic							
Ordered[92]	–	0.054	0.258	0.462	0.140	0.077	0.009
Disordered[92]	–	0.097	0.340	0.262	0.233	0.039	0.010
	(0.010)						
Wax Convect.[147]	–	0.023	0.357	0.377	0.220	0.023	

TABLE 7, *continued*

System	$\rho(3)$ ($\rho(10)$)	$\rho(4)$ ($\rho(11)$)	$\rho(5)$ ($\rho(12)$)	$\rho(6)$ ($\rho(13)$)	$\rho(7)$ ($\rho(14)$)	$\rho(8)$ ($\rho(15)$)	$\rho(9)$ ($\rho(16)$)
				Experiment			
Two D Sections of 3 D Materials							
Froths							
Polyurethane Foam[250]	0.049 (0.002)	0.145	0.229	0.318	0.175	0.067	0.016
Metal Grains							
Tin							
Champur[64]	0.100 (0.008)	0.227 (0.005)	0.290 (0.003)	0.206 (0.001)	0.097	0.043	0.019
Aluminum							
High Purity	0.038 (0.019)	0.161 (0.009)	0.256 (0.005)	0.250	0.148	0.076	0.039
Pure 500° C[24]							
1m	0.014 (0.020)	0.152 (0.009)	0.261 (0.001)	0.267	0.156	0.074	0.047
25m	0.023 (0.012)	0.167 (0.005)	0.257 (0.005)	0.253	0.149	0.096	0.035
125m	0.073 (0.008)	0.198 (0.005)	0.286 (0.005)	0.230	0.114	0.048	0.034
625m	0.029 (0.031)	0.146 (0.012)	0.251 (0.009)	0.225	0.174	0.071	0.053
Average	0.035 (0.018)	0.166 (0.008)	0.264 (0.005)	0.244	0.148	0.072	0.042
±	0.026 (0.010)	0.023 (0.003)	0.015 (0.003)	0.019	0.025	0.019	0.009
α Iron[206]	0.063	0.083	0.104	0.396	0.271	0.063	0.021
β-Brass[206]	0.025	0.202	0.436	0.287	0.046	0.007	
Ceramics							
Blanc *et al.*[30]							
Al_2O_3 Uncorrected	0.04 (0.02)	0.17 (0.01)	0.29	0.21	0.12	0.10	0.04
Corrected	0.036 (0.024)	0.158 (0.013)	0.276	0.213	0.127	0.108	0.045

TABLE 7, *continued*

System	$\rho(3)$ ($\rho(10)$)	$\rho(4)$ ($\rho(11)$)	$\rho(5)$ ($\rho(12)$)	$\rho(6)$ ($\rho(13)$)	$\rho(7)$ ($\rho(14)$)	$\rho(8)$ ($\rho(15)$)	$\rho(9)$ ($\rho(16)$)
Experiment							
Two D Sectns of 3 D Mats							
Ceramics							
Sintered Alumina[137]	0.021 (0.009)	0.153 (0.007)	0.258 (0.001)	0.281	0.131	0.131	0.100
Corrected	0.018 (0.010)	0.141 (0.008)	0.246 (0.001)	0.281	0.140	0.111	0.044
MgO + LiF[9] $N = 9906$	0.024 (0.013)	0.160 (0.005)	0.279 (0.0013)	0.248	0.155	0.081	0.034
Biological Materials							
Vegetable Cells[206]	0.051	0.273	0.397	0.254	0.063	0.008	0.001
Theory							
Geometrical Models							
Pure Geometrical							
Voronoi[34] $N = 1377$	0.012 (0.008)	0.105 (0.0007)	0.264 (0.0007)	0.295	0.197	0.088	0.031
$N = 57,000$[52]	0.0110 (0.0075)	0.1078 (0.0014)	0.2594 (.00018)	0.2952 (.00005)	0.1984	0.0896	0.0296
Clumped	0.013	0.108	0.266	0.289	0.192	0.079	0.041
Relaxed[105] $N = 1366$	– (0.011)	0.022 (0.0007)	0.258 (0.0007)	0.467	0.211	0.037	0.006
Glass Models[204]							
Triangle Raft	–	0.062	0.256	0.392	0.196	0.095	
Triangle-Line Raft	0.009 (0.004)	0.078	0.245	0.363	0.183	0.107	0.010
2 D Sectns of 3 D Arrays[250]							
Pentagonal Dodecahedra	0.089 (0.008)	0.128	0.212	0.293	0.204	0.061	0.007
Tetrakaidecahedra	0.073 (0.011)	0.134	0.118	0.3144	0.185	0.130	0.037
Coordination # 4							
Poisson[191]	0.354	0.377	0.191	0.059	0.009		

TABLE 7, *continued*

System	$\rho(3)$ ($\rho(10)$)	$\rho(4)$ ($\rho(11)$)	$\rho(5)$ ($\rho(12)$)	$\rho(6)$ ($\rho(13)$)	$\rho(7)$ ($\rho(14)$)	$\rho(8)$ ($\rho(15)$)	$\rho(9)$ ($\rho(16)$)
				Theory			
Maximum Entropy							
Kikuchi I[121]	0.035 (0.015)	0.141 (0.001)	0.233	0.238	0.185	0.107	0.045
Kikuchi II	0.025 (0.009)	0.107 (0.001)	0.243	0.274	0.189	0.109	0.042
Almeida *et al.*[10]	0.210 0.035	0.195 0.025	0.159 0.018	0.118 0.013	0.086 0.009	0.063 0.007	0.047
Vertex Models							
Weaire *et al.*							
"Exact"[244]	– (0.008)	0.145	0.251	0.261	0.194	0.103	0.038
"Exact"[243]	0.003 (0.003)	0.078	0.259	0.358	0.200	0.091	0.008
Soares *et al.*[210] Straight Sides	0.027 (0.009)	0.149	0.229	0.223	0.198	0.125	0.040
Kawasaki *et al.*[259]							
Model I	0.054 (0.027)	0.153 (0.010)	0.236 (0.005)	0.216 (0.002)	0.151	0.091	0.055
Model II	0.031 (0.019)	0.141 (0.006)	0.253 (0.002)	0.237	0.173	0.094	0.045
Enomoto *et al.*[62]	0.068 (0.023)	0.134 (0.014)	0.255 (0.005)	0.213 –	0.147 (0.005)	0.082	0.053
Mean Field Theories							
Marder[157]	0.011 (0.015)	0.076 (0.008)	0.263 (0.006)	0.414	0.123	0.056	0.029

TABLE 7, *continued*

System	$\rho(3)$ ($\rho(10)$)	$\rho(4)$ ($\rho(11)$)	$\rho(5)$ ($\rho(12)$)	$\rho(6)$ ($\rho(13)$)	$\rho(7)$ ($\rho(14)$)	$\rho(8)$ ($\rho(15)$)	$\rho(9)$ ($\rho(16)$)
				Theory			
Network Models							
Fradkov *et al.*[76]							
T1's per T2	0.002	0.046	0.288	0.390	0.193	0.064	0.016
0	(0.002)						
1	0.018	0.115	0.262	0.273	0.184	0.089	0.033
	(0.010)	(0.003)					
2	0.048	0.145	0.224	0.222	0.158	0.099	0.046
				[$\rho(2)$]			
	(0.022)	(0.009)		[0.010]			
10	0.127	0.145	0.145	0.135	0.110	0.080	0.046
	0.033	0.022		[0.073]			
∞	0.127	0.107	0.093	0.077	0.065	0.053	0.049
	(0.038)	(0.032)		[0.152]			
Potts Model							
Potts Model[93]	0.025	0.128	0.271	0.253	0.161	0.084	0.039
Triangle Lattice	(0.019)	(0.008)	(0.003)				

TABLE 7, *continued*

System	$\rho(3)$ ($\rho(10)$)	$\rho(4)$ ($\rho(11)$)	$\rho(5)$ ($\rho(12)$)	$\rho(6)$ ($\rho(13)$)	$\rho(7)$ ($\rho(14)$)	$\rho(8)$ ($\rho(15)$)	$\rho(9)$ ($\rho(16)$)
			Theory				
Two D Sect of 3 D Mat							
Carnal & Mocellin[46]							
$\beta = 0$	0.297 (0.029)	0.190 (0.022)	0.129 (0.018)	0.092 (0.014)	0.067 (0.011)	0.050	0.038
$\beta = 2$	0.065 (0.028)	0.174 (0.015)	0.222 (0.008)	0.205 (0.004)	0.138 (0.002)	0.086	0.050
$\beta = 4$	0.011 (0.013)	0.118 (0.005)	0.264 (0.002)	0.297 (0.001)	0.171	0.083	0.035
$\beta = 6$ (T1 rate)	0.002 (0.006)	0.070 (0.001)	0.273	0.373	0.184	0.069	0.021
Blanc & Mocellin[30]							
	0.036 (0.025)	0.173 (0.009)	0.231 (0.003)	0.215 (0.0008)	0.154	0.099	0.054
Depends on $\rho(3)$ as	0.100 (0.033)	0.146 (0.013)	0.194 (0.004)	0.194 (0.001)	0.151	0.101	0.064
a parameter no T1's	0.050 (0.026)	0.169 (0.009)	0.227 (0.003)	0.212 (0.0006)	0.155	0.104	0.056
	– (0.021)	0.190 (0.006)	0.259 (0.0009)	0.230	0.160	0.094	0.050
Kurtz & Carpay[132]							
Potts Model[15]							
	0.076 (0.027)	0.185 (0.010)	0.230 (0.005)	0.212 (0.004)	0.121 (0.002)	0.082 (0.001)	0.046

TABLE 8

SIDE DISTRIBUTION MOMENTS

System	$< n >$	μ_2	μ_3	μ_4	W
Experiment					
2-D Soap Froth					
Smith[121]	5.928	1.759	1.148	10.21	1.005
Smith[259]	5.94	1.296	0.114	4.30	0.877
Aboav[8]					
$t = 0$ hours $N = 4612$	5.988	0.242	0.003	0.26	0.249
$t = 0$ hours $N = 5687$	5.990	0.620	-0.011	1.38	0.519
$t = 15$ hours $N = 3550$	5.968	0.976	-0.068	3.56	0.687
$t = 30$ hours $N = 3623$	5.993	1.30	0.486	6.00	0.827
$t = 75$ hours $N = 1372$	5.982	1.98	1.763	15.62	1.028
$t = 105$ hours $N = 584$	6.010	2.86	8.153	76.10	1.247
Glazier *et al.*					
Air[93]	5.999	2.490	2.490	26.66	1.144
Air $N = 343$[94]	5.935	1.492	1.090	8.623	.925
Air $N = 111$	5.910	1.523	1.295	7.113	.951
Helium $N = 1696$	5.983	2.151	3.933	24.29	1.045
Helium $N = 423$	5.972	1.437	1.017	6.01	0.927
Helium $N = 311$	5.915	1.491	1.017	6.87	0.958
Average of Above	5.952	1.764	1.980	13.26	0.992
$\pm$	0.037	0.445	1.366	9.53	0.0087
Metal Grains					
Al + 10^{-4} Mg .22mm Foil[75]					
$t = 0$ hours	5.975	2.993	5.824	49.58	1.277
$t = 1.5$ hours	5.835	2.353	1.921	18.24	1.210
$t = 3.25$ hours	5.916	2.465	2.644	20.97	1.214
$t = 4.25$ hours	6.091	3.791	9.257	84.07	1.414
Average of Above	5.952	2.900	5.013	43.90	1.269
Biological Systems					
Cucumber[142]	5.998	0.748	0.137	1.62	0.619
Dividing Cucumber[147]	6.992	0.656	0.092	1.23	0.570
Eupatorium[147]	5.992	0.752	0.082	1.55	0.629
Human Amnion[142]	5.987	1.00	0.068	3.02	0.734
Mouthbreeder Fish[105]	5.929	0.352	0.004	0.35	0.398

TABLE 8, *continued*

System	$< n >$	μ_2	μ_3	μ_4	W
Experiment					
Rock Fracture[191]					
Giant's Causeway	5.702	0.596	0.165	1.33	0.624
Devil's Postpile	5.448	0.733	-0.325	1.80	0.719
Mt. Rodeix	5.228	0.522	0.005	0.69	0.592
Devil's Tower	5.296	0.657	0.019	1.03	0.687
Europa Type 1,2	5.161	0.858	-0.018	2.14	0.708
Coördination # 4 Rock Fracture[191]					
Circle Cliffs	3.720	0.297	-0.008	0.22	0.473
Zendan, Iran	3.671	0.392	0.144	0.52	0.545
Colorado	3.696	0.252	-0.046	0.14	0.451
Europa Type 3	3.739	0.495	0.198	0.67	0.596
Europa Mixed	4.243	0.791	0.553	2.69	0.692
Other 2-D Systems					
Photo Emulsion $N = 1000$[142]	6.00	4.344	12.402	111.66	1.580
Lipid Monolayers					
Stearic Acid[169]	5.836	3.309	7.705	66.37	1.313
Ordered[92]	5.955	1.001	0.444	3.29	0.704
Disordered[92]	5.874	1.432	1.125	7.28	0.958
Wax Convection[147]	5.863	0.742	0.171	1.32	0.702
Two D Sections of 3 D Materials					
Froths					
Polyurethane Foam[250]	5.697	1.771	0.172	8.70	1.076
Metal Grains					
Champur Tin[64]	5.278	5.278	4.074	30.62	1.200
High Purity Aluminum[64]	5.877	2.746	3.739	29.40	1.271
Pure Aluminum at 500° C[24]					
1 minute	5.967	2.445	3.047	21.68	1.188
25 minutes	5.883	2.440	2.849	22.48	1.216
125 minutes	5.500	2.534	3.779	28.64	1.243
625 minutes	6.081	3.118	4.534	35.33	1.362
α Iron[206]	6.000	1.708	-1.125	9.46	0.917
β-Brass[207]	5.148	0.812	0.781	2.03	0.698

TABLE 8, *continued*

System	$< n >$	μ_2	μ_3	μ_4	W
Experiment					
Ceramics					
Blanc and Mocellin Al_2O_3[30]					
Uncorrected	5.82	2.748	3.290	24.41	1.32
Corrected	5.939	2.901	3.386	26.25	1.343
Sintered Alumina uncorrected[137]	5.895	2.278	2.269	18.02	1.164
Sintered Alumina corrected[137]	5.998	2.348	2.226	18.31	1.162
MgO + LiF flux $N = 9906$[9]	5.835	2.279	2.415	18.51	1.188
Biological Materials					
Vegetable Cells[206]	5.032	1.022	0.244	3.07	0.760
Theory					
Geometrical Models					
Pure Geometrical					
Voronoi $N = 1377$[34]	6.00	1.79	1.089	10.41	1.014
Voronoi $N = 57,000$[52]	5.997	1.777	1.026	10.68	1.013
Negative Binomial Voronoi[34]	6.00	1.91	1.367	11.97	1.047
Relaxed Voronoi[105]	6.000	0.754	0.222	1.858	0.603
Coörd. # 4 Poisson[191]	3.981	0.869	0.604	2.28	0.702
Glass Models[204]					
Triangle Raft	6.007	1.079	0.185	2.95	0.768
Triangle-Line Raft	6.015	1.409	0.400	6.01	0.879
2-D Sections of 3-D Arrays					
Pentagonal Dodecahedra[250]	5.646	2.032	-0.032	11.61	1.162
Tetrakaidekahedra	5.993	2.506	-0.212	16.03	1.202
Topological Transforms					
Kikuchi I[121]	5.982	2.399	1.208	15.51	1.223
Kikuchi II	6.041	2.072	0.876	12.22	1.120
Maximum Entropy Models					
Almeida *et al.*[10]	5.98	∞	∞	∞	2.130(?)
Vertex Models					
"Exact"[244]	6.005	1.907	1.116	9.516	1.089
"Exact"[243]	5.996	1.286	0.403	4.86	0.844
Soares *et al.*[210]	5.997	2.273	0.740	12.63	1.213

TABLE 8, *continued*

System	$< n >$	μ_2	μ_3	μ_4	W
Theory					
Vertex Models					
Kawasaki *et al.*[259]					
Model I	5.993	3.277	4.085	36.41	1.401
Model II	5.979	2.544	2.288	20.75	1.239
Enomoto *et al.*[62]	5.980	3.609	6.390	57.50	1.437
Mean Field Theories					
Marder[157]	6.005	1.909	3.287	21.57	0.905
Network Models					
Fradkov *et al.*[76] T1's per T2					
0	5.991	1.111	0.560	4.14	0.765
1	5.554	2.758	0.983	20.36	1.358
2	5.929	2.984	2.089	26.56	1.357
10	5.502	5.170	5.129	66.72	1.886
∞	5.159	7.136	11.168	114.65	2.254
Beenakker[25]	6.00	max=3.2 final=0.25			
Potts Model					
Potts Model[93]	5.978	2.490	2.971	23.22	1.196
Two D Sections of 3 D Mater.					
Blanc and Mocellin[30]					
$\rho(3) = 0.036$	5.264	3.969	5.172	44.41	1.654
$\rho(3) = 0.100$	5.984	3.839	3.660	41.45	1.558
$\rho(3) = 0.050$	5.989	3.174	3.300	30.78	1.403
$\rho(3) = 0.000$	5.976	2.489	2.881	19.18	1.244
Carnal and Mocellin[46]					
$\beta = 0$	5.37	7.156	24.918	206.69	2.120
$\beta = 2$	5.97	3.881	6.921	59.42	1.510
$\beta = 4$	6.005	2.107	2.475	18.77	1.073
$\beta = 6$	5.995	1.342	0.946	6.73	0.835
Kurtz and Carpay[260]	5.748	2.308	0.992	12.91	1.253
3 D Potts Model[15]	5.830	3.736	7.189	61.80	1.492

and found them identical within experimental error, thus showing that the distribution was indeed time invariant. We give Glazier *et al.*'s measurement for the scaling distribution in Fig. 35.

Smith's data for the two dimensional froth had $\mathcal{R} < 1$ (See Table 7), suggesting that he never saw a fully equilibrated froth. His actual distributions were not too different from those of Stavans and Glazier, however, considering the large counting error in his small sample. His measured growth exponent of $\alpha = 1$, on the other hand, suggests that he did observe a scaling state. If his side distribution came from early in the run (he never indicates when he made the measurement), it would resolve the apparent contradiction. Aboav observed the same sequence of events, with $\mathcal{R}$ increasing monotonically, and the large n tail of the distribution broadening (See Table 7), but, as we noted in discussing his value for the growth exponent, stopped his measurement just before the froth reached its scaling state (only his last data point had $\mathcal{R} > 1$) so he did not observe the subsequent narrowing and equilibration of the distribution.

In Fig. 36 we show evidence from Stavans and Glazier, that the scaling state is universal for the soap froth. They measured the second moment versus time for an initially ordered helium froth (that shown in Fig. 16 (d) and 9 (a)) and an initially disordered air froth (that shown in Fig. 16 (f) and 9 (b)). The initially ordered froth started with a very small μ_2 which increased rapidly to a maximum value of $\mu_2 = 2.65$, (at about 9 hours, corresponding to Fig. 16 (d) point D and Fig. 9 (D)) at the time when the rate of area

increase was maximal. μ_2 then dropped rapidly, reaching a constant value of $\mu_2 = 1.4 \pm 0.1$, at around 15 hours when the rate of growth rolled over into a power law (Fig. 16 (d) point E and Fig. 9 (E)). In the initially disordered froth the value of μ_2 first dropped for about five hours (thus confirming the initial drop in ∂ shown in Fig. 16 (f)). At these early times there were many bubbles and the moment estimates were sufficiently accurate that the drop cannot be a counting error fluctuation. μ_2 then recovered, reaching a constant value of $\mu_2 = 1.4 \pm 0.1$, at around 50 hours when the rate of growth rolled over into a power law (Fig. 16 (f) point C' and Fig. 9 (C')). Thus the final value of μ_2 was independent of the diffusing gas and of the initial configuration of the froth. In both cases the scatter increased as the number of bubbles decreased at long times. There was no evidence of any significant trend at long times, the slight decrease in the last few values of μ_2 apparently occurring when the expected number of nine-sided bubbles dropped below one. If we reject these points, our estimate of the equilibrium value of μ_2 would increase slightly to $\mu_2 = 1.45 \pm 0.1$ for both the initially ordered and initially disordered froths. In contrast, Aboav observed a monotonic increase in μ_2 from 0.242 to 2.86, as we would expect for observations made during the froth's equilibration (See Tables 7 and 8).

We show the same quantities calculated by Glazier *et al.* (for the air froth shown in Fig. 17) in Fig. 37. The scatter is larger than in Fig. 36 because they analyzed only a 30% sample of the total experimental image. The last few points represent only about six bubbles each. Digitization errors also

resulted in the creation of some spurious many- and few-sided bubbles. The distributions were rechecked by hand, but some errors doubtless remained to contribute to the scatter. We observe the same basic pattern as in Fig. 36. The initially narrow distribution (small value of μ_2) widened to a maximum width of $\mu_2 \approx 3.25$, then narrowed to a stable value of $\mu_2 = 1.6 \pm 0.2$, in agreement with the value of Stavans and Glazier, at the same time as the rate of area growth rolled over into a power law ($\approx 10,000$ minutes, see Fig. 17).

The higher moments behaved similarly. We have calculated the evolution of μ_3 (Fig. 38), μ_4 (Fig. 39) and W (Fig. 40) from the data of Glazier *et al.*. The third moment, which measures the asymmetry of the distribution, in this case mostly the strength of the large n tail, began near zero, increased rapidly to a maximum during equilibration when the frequency of many-sided bubbles was maximal ($\mu_4 \approx 4.5$), then dropped to a stable value of $\mu_3 = 1 \pm 0.5$. The graph suggests that μ_3, may have undergone a second oscillation, undershooting the stable value around 10,000 minutes and reaching a second slightly lower maximum of $\mu_3 \approx 2.5$ around 20,000 minutes. If so, it is a surprising confirmation of the prediction by Beenakker that equilibration should require multiple oscillations.[25] Nothing changes if we look at the fourth moment which represents the flatness of the distribution, essentially the relative strength of $\rho(4)$, $\rho(7)$, and $\rho(8)$ versus $\rho(5)$ and $\rho(6)$. The initial value was $\mu_4 \approx 5$. It then grew to $\mu_4 \approx 40$ and decreased, with a possible oscillation and second peak at 20,000 minutes, to a stable value of $\mu_4 =$

6 ± 3.5. We call the initial maximum in all the distribution functions, the **equilibrating maximum.**

We might speculate that the second maximum we observe in the third and fourth moments represents the decay of next nearest neighbor correlations while the first peak represents the decay of nearest neighbor correlations. In that case the time between the peaks would represent the time for an average bubble to disappear, and hence for disorder to propagate a distance of one bubble radius. The oscillation might also result from a phase lag caused by different time constants for area and side equilibration. However, without experimental values for μ_3 and μ_4 from other experimental runs (in particular those of Stavans and Glazier), we must presume that the apparent oscillation is a statistical artifact, which could result if, for example, a single very many-sided bubble appeared at roughly 15,000 minutes and gradually began to shed sides after 20,000 minutes. We mention this scenario as an example only, since we see no single many-sided bubble in the data to throw off our calculations.

The width (Fig. 40) increased from an initial minimum of $W \approx 0.4$ to a stable value ($W = 1.1 \pm 0.3$) at around 10,000 minutes, with a possible weak maximum of $W \approx 1.3$ at 5000 minutes. Any oscillation at 20,000 minutes was lost in noise.

Returning to our comparison of Glazier *et al.*'s results to those of Smith and Aboav: Smith's original distribution came within one standard deviation of the Glazier *et al.* values for all moments, suggesting that he was reasonably

close to equilibrium.[206] The distribution given by Kikuchi, however, gives unexpectedly low values for all moments, suggesting that it was taken early in a run before the initial equilibrating maximum. If we look at Aboav's final state at $t = 105$ hours, we find elevated values of all moments as expected near the equilibration maximum.

In Table 7 we summarize side distributions for the soap froth, several biological systems, metallic grain growth, rock fracture, and several other systems, as well as many of the models we have discussed. We give corresponding moments in Table 8. We note that in this table we give the moments exactly as calculated from the published distributions, even when it is clear that the exact distribution would give infinite values for the higher moments.

In spite of the large scatter in our measurements, the scaling state side distribution of the soap froth is surprisingly difficult to match theoretically. As typical froth distributions we take the averaged long time distributions of Glazier *et al.* (the first line in the appropriate section of Table 7) and an average of unpublished data of Glazier and data of Stavans and Glazier (the last line of the appropriate section in Table 7) . None of the geometrical models is within range, nor are the maximum entropy models of Rivier, Kikuchi, or Almeida and Iglesias. Among the topological mean field theories, Marder's model is generally within range, but gives an excessively high value of μ_3 because of its correlated side redistribution which tends to make many-sided bubbles gain sides and thus stretches the large n tail. Blanc and

Mocellin's model for two dimensional growth (no nucleation of three-sided bubbles) is equally tail heavy. Fradkov, Shvindlerman and Udler's network model has difficulty matching both μ_2 and μ_3 for a given rate of side swapping, but does a reasonable qualitative job. Kawasaki's vertex Model II does reasonably well with the moments but has far too many four-sided bubbles. Weaire and Kermode's vertex model never reached equilibrium and Frost and Thompson never published side distributions for their boundary dynamics model so we have no data for comparisons from the two most physically appealing "exact" models. The boundary dynamics model of Soares, Ferro and Fortes is very tail heavy.

We plot the side distribution for the hexagonal lattice Potts model in Fig. 35. Referring to Table 7 we find that the predicted values for the $\rho(n)$ are within the measured experimental scatter for all n, though the averaged froth distribution has fewer four- and many-sided bubbles. Looking at the moments, we find that the Potts model again gave consistently larger values than the averaged froth, though within the experimental scatter in all cases. If we compare to the distribution from Glazier *et al.*, the agreement is much better: exact for μ_2 and within 10% for all other moments, with μ_3 a little high, as we expect from the stretched tail.

If we try to match the froth to other experimental coarsening patterns the only experiment that provides a reasonable match is Fradkov, Shvindlerman and Udler's measurement of two dimensional grain growth in Al $+10^{-4}$ Mg foil. The side distributions are similar in shape with $\mathcal{R} = 1.05$ for the

grain growth and $\mathcal{R} = 1.03$ for the froth. The chief difference is the prominence of the tail in the metallic grain growth. Nevertheless, because of the large scatter in both measurements, the measured range of distributions and moments overlap in all categories. Unsurprisingly, Fradkov, Shvindlerman and Udler's network model with the rate of $T1$'s set to be about 5 times the rate of $T2$'s agrees well with their experimental data for the foil. The Potts model also is within range of the results for the foil for all values, though consistently on the low side for the moments.

The apparent failure of topological mean field theories and network models to predict the moments in the soap froth correctly is surprising– but given the large uncertainties in the experimental distributions hardly conclusive. There may be an anti many-sided bubble bias built into the soap froth. Perhaps, we need to include an anticorrelation in side shedding: that many-sided bubbles preferentially lose sides and few-sided bubbles preferentially gain sides, a possible source for this anticorrelation being the deviation of internal angles from the predicted 120°. Another factor may be statistical. Theoretical distributions are usually calculated for large samples, and thus avoid the anti many-sided bias that we have noted in the experimental data.

In the case of the Potts model and metallic grain growth the discrepancy may arise from stiffness caused by anisotropy. The excess curvature which opposes increases in number of sides for many-sided bubbles is masked in the presence of anisotropy. In this case we would expect that the third moment would increase with increasing anisotropy. Unfortunately we have no

data on the dependence of the distribution functions on the relative orientational anisotropies of the Potts model and metal films, though it would be straightforward to design an experiment to test the hypothesis. In particular, for lower anisotropies and higher temperatures, the frequency of many-sided bubbles should decrease. An additional factor may come from the relative rates of diffusion along and across grain boundaries. We expect that the Potts model and metal grains will be further from equilibrium than a soap froth, and hence may eliminate many sided bubbles more slowly, since a bubble may not "know" how many sides it really has. Again, careful measurements using different materials and temperatures could test the hypothesis. Any theory must explain why the metal film gives a larger tail than the Potts model.

We tentatively assert the existence of a universal distribution function for two dimensional coarsening including the soap froth, two dimensional grain growth in metals and the Potts model. It seems that the soap froth has a lower frequency of many-sided bubbles than the Potts model, and the Potts model than real grain growth. However, with our current data we cannot really distinguish the three cases. In particular we have no way to determine whether a larger or smaller frequency of many-sided bubbles is "ideal." We cannot tell whether disequilibria or anisotropies in the Potts model cause a deviation from the ideal coarsening of the soap froth, or whether an anti many-sided bubble bias causes the soap froth to deviate from the ideal coarsening of the Potts model. The mean field and network models may also

belong to this class if proper side shedding anticorrelations are included. All our speculation may be premature, however, since our current poor experimental accuracy cannot distinguish any given soap froth distribution from a Potts model distribution or a metal film distribution. We certainly need better experimental data, especially scaling states for the soap froth with many (i.e. thousands) of bubbles.

Proceeding down our list of experimental categories we come to two dimensional biological systems. Bénard-Marangoni convection patterns in wax also belong in this group. These have narrow side distributions, tightly and symmetrically centered around $n = 6$, with $\mathcal{R} = 0.45 \pm 0.2$, μ_2 between 0.35 and 1, $\mu_3 < 2$, $\mu_4 < 3$ and W between 0.4 and 0.7. The sharp cutoffs in the distributions at $n = 4$ and $n = 7$ are distinctive. The dividing cucumber cells are a special case since they represent a selection rather than an entire pattern, as the large value for $< n >$ shows. We have no difficulty distinguishing these distributions from two dimensional coarsening. The models that work for these systems are the pure geometrical constructions, particularly the relaxed Voronoi, which gives excellent agreement. The network model of Fradkov, Shvindlerman and Udler with no $T1$'s to redistribute sides is also not too far off. In both the models and the experiments the basic physics seems clear. The mobility of cells and territories is small and their area range limited (if they grow too large they split, if too small they die and disappear). The pattern can readjust locally to eliminate stress, but diffusive equilibration does not occur.

Fracture patterns in rock belong to the same non-equilibrating class, with distributions composed almost entirely of five-, six- and seven-sided bubbles. $\mathcal{R}$ ranges from 0.7 for the Giant's Causeway to 1.8 for cracks on Europa, but the moments stay small, with $\mu_2 = 0.6 \pm 0.2$, $\mu_3 = 0 \pm 0.2$, $\mu_4 \approx 1.4 \pm 0.6$ and $W \approx 0.6 \pm 0.1$. Once again we have no trouble distinguishing such patterns from two dimensional coarsening. The models described for biological systems work for geological as well. A slight complication are the various coördination number four patterns whose distribution functions are radically different from the others but which give similar moments to coördination number three fracture, suggesting that the non-relaxational physics is similar in the two cases. It also serves as a warning not to accept similarity of moments as definitive without looking at the actual distribution functions.

We next come to two polymer systems. The photo emulsion has frozen in a broad area distribution generated by a spray from a nozzle. The lipid monolayer began with a similarly broad area distribution but had time to at least partially equilibrate diffusively. The emulsion distribution is exceptionally broad, with $\mathcal{R} = 1.5$, and $\rho(4) > \rho(6)$, with a tail extending to $n = 19$. The monolayer is less extreme, with $\mathcal{R} = 1$, $\rho(4) = 0.125$, and a cutoff at $n = 13$. The moments are correspondingly large and are well separated from those of two dimensional coarsening. We are clearly in a regime where side exchange is a dominant process, and our best agreement with models comes from Fradkov, Shvindlerman and Udler's high $T1$ rate network model (∞ or 10 $T1$'s per $T2$), or the mean field theory of Blanc and Mocellin in the same

limit ($\beta = 0$ or $\beta = 2$). Again, the physical motivation seems clear. The well separated drops can move freely, and easily slide past one another to reduce stress. However their large separation results in slow diffusion rates, hence the failure to reach equilibrium. We will discuss the equilibration of lipid monolayers in a later chapter.

Finally we consider two dimensional sections of three dimensional systems. If we neglect Smiths's measurements for α-iron, a reasonably consistent picture emerges for grain coarsening. The constancy of Beck's measurements of the distributions in aluminum as a function of time suggests that we are safe to assume that the all metallic distribution functions are in scaling states. Taking a rough average over the various metals and ceramics we obtain a "typical" three dimensional coarsening distribution with $\mathcal{R} \approx 1$, $\rho(3) \approx 0.04$, with a relatively long tail, $\rho(9) \approx 0.05$ and $\rho(10) \approx 0.02$. The moments are quite consistent, with $\mu_2 \approx 2.6 \pm 0.2$, $\mu_3 \approx 3.5 \pm 1.5$, $\mu_4 \approx 25 \pm 5$, and $W \approx 1.3 \pm 0.2$. The moments for the polyurethane foam are slightly smaller, probably because its initial condition consisted of nearly uniform volumes and it cured before reaching equilibrium. The vegetable cells, where, as we have discussed, both areas and mobility are constrained, also show lower moments. The poor value of $< n >= 5$ warns us to be cautious in interpreting the vegetable cell data, but both the froth and the cells are in reasonable agreement with the sectioning of a *regular* array of tetrakaidekahedra or dodecahedra, which is reasonable if they are relaxed close packings of nearly equal volume bubbles. The agreement between random and regular

structures also reminds us just how much information is lost taking a two dimensional section of a three dimensional structure.

Two dimensional coarsening distributions and three dimensional coarsening distributions are clearly distinct. The best results for the three dimensional distributions come from the mean field theories of Blanc and Mocellin and Carnal and Mocellin which were designed precisely for this purpose.[30,46] Interpolating for $\rho(3) \approx 0.04$ and $\beta \approx 3$ respectively fits the distribution and all the moments to well within the experimental error. The actual distribution function of the Carnal and Mocellin model is particularly impressive. The three dimensional Potts model gives values of moments much too large and a tail much more extended than our hypothetical "typical coarsening." Whether this disagreement results from finite size or anisotropy effects, or the particular choice of comparisons (we note that the comparisons given in the paper of Anderson, Grest and Srolovitz fit only marginally better),[15] is unclear.

There does seem to be a typical side distribution for two dimensional sections of three dimensional grain growth (and hence, presumably for three dimensional grain growth itself). It is striking that the simplest of topological mean field theories, which assumes no side shedding correlations and independent creation and destruction of three-sided bubbles, and which requires only one rate constant, seems perfectly adequate to describe all of the measured patterns in three dimensions. In two dimensions, on the other hand, none of our theories is entirely satisfactory, and the one that works the

best is also the most complicated and microscopically detailed. As in two dimensions, structures with limited area distribuitions have distinctly different side distributions. The range of scatter in the distributions is narrower in three dimensions than in two, as if the details of what was coarsening mattered less (this is partly an effect of the loss of information from taking a section, but we are still perfectly able to distinguish coarsening from non-equilibrating cellular aggregates and foams). The extra dimension seems to reduce the effects of topological constraints, anisotropy, etc., and paradoxically to simplify the physics, while making exact modeling more difficult.

VI.b Area Distributions

Because we have much less reliable data on the equilibrium area distribution of the soap froth, we will treat the topic of area distributions more briefly than the side distributions, focusing on comparisons to the Potts model simulation. In particular we lack the distributions of bubble radii which are the probabilities calculated by most models. We will not quote the many distribution functions available for metals. We refer the interested reader to the papers of Beck or Anderson *et al.*.[15,24]

If we examine the time evolution of Glazier *et al.*'s area histograms (Fig. 41) for the two dimensional soap froth, $\rho(A/ < a >)$, we find roughly the same scenario that we found for side distributions. At short times the distribution peaks sharply around the average area (corresponding to a pattern composed primarily of uniform sized six-sided bubbles). In time, the most probable size gradually decreases to zero while the large area tail of the dis-

Fig. 41 Area Distribution versus Time. Evolution of the area distribution for an initially ordered two dimensional air froth. Times are: (a) $t = 0$ minutes. (b) $t = 545$ minutes. (c) $t = 1124$ minutes. (d) $t = 1565$ minutes. (e) $t = 2044$ minutes. (f) $t = 3163$ minutes (From Glazier *et al.*1989).[93]

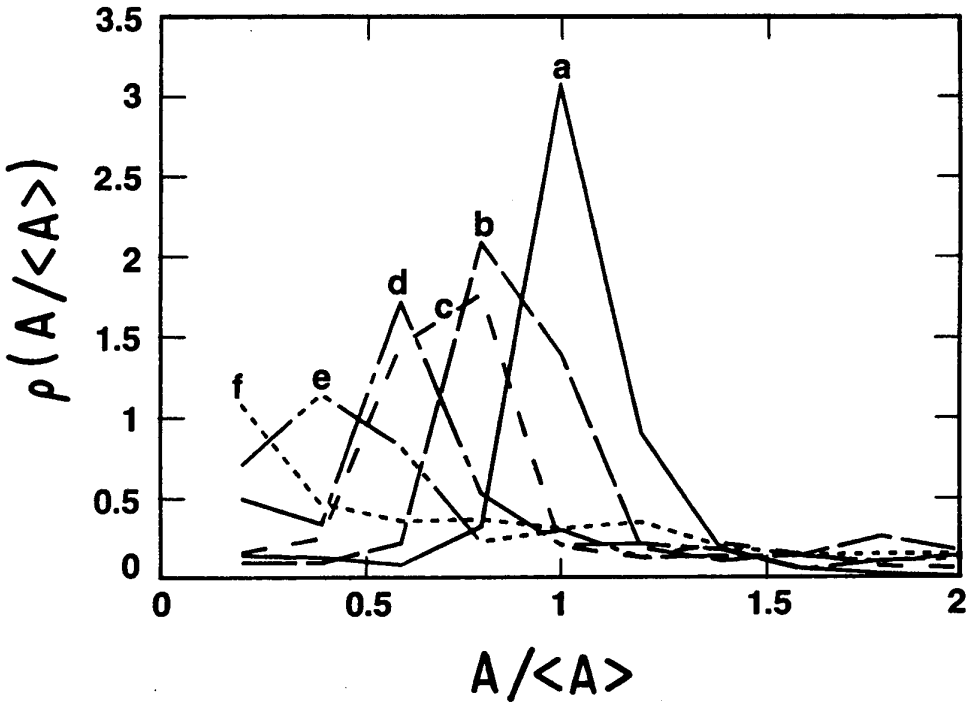
3.5
3
2.5
2
1.5
1
0.5
0
0
0.5
1
1.5
2
ρ(A/<A>)
A/<A>
a
b
c
d
e
f

Fig. 42 Correlated Area Distributions. Area distributions for five-, six-, seven- and eight-sided bubbles in the scaling state. Measurements in air froth (solid line) and Potts model with identical starting conditions (heavy dashed line). Total area distributions are shown for reference for the soap froth (dotted line) and Potts model (light dashed line) (From Glazier *et al.* 1989).[93]

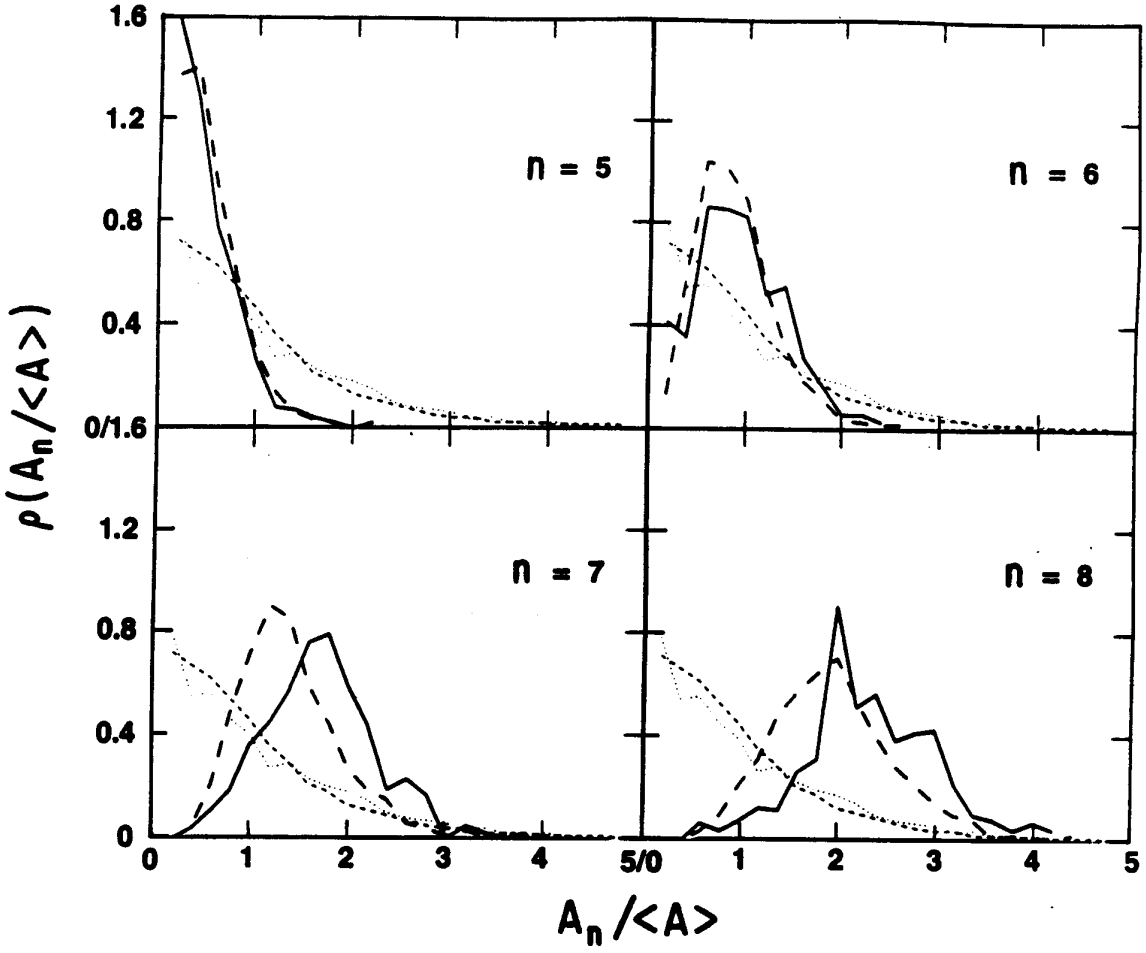
1.6
1.2
0.8
0.4
0/1.6
1.2
0.8
0.4
0
0
1
2
3
4
5/0
1
2
3
4
5
n = 5
n = 6
n = 7
n = 8
ρ(A_n/<A>)
A_n /<A>

tribution gradually lengthens. This broadening comes about because the fraction of shrinking small bubbles with near zero absolute area remains essentially constant, while their relative size decreases as the total length scale increases. Eventually the distribution reaches a time invariant scaling state.

We next examine the scaling state distributions more closely. In Fig. 42 we plot Glazier *et al.*'s area distributions for five-, six-, seven-, and eight-sided bubbles and compare them to the total distribution functions and the equivalent results from the Potts model simulation. As we might expect for bubbles which shrink, the most probable area for a five-sided bubble is zero, agreeing with the Potts model result. Six-sided bubbles have a relatively narrow width around the average area, with good agreement between the experiment and the Potts model. Both seven- and eight-sided bubbles are larger, with broader distributions than the six-sided bubbles. The Potts model seems to give a higher third moment than the actual froth for these types (again we may suppose that this is an anisotropy effect), but the difference is statistically significant only for seven-sided bubbles.

Comparing to other models we find comparable distributions from the various mean field theories, network models and boundary dynamic models. Unfortunately, the error in our measurement of the area distribution and the difficulty of determining exactly how the histograms were constructed, makes the area distribution useless as a diagnostic.